

## Chapter 7

# First Experiments with the BEC-CQED System

While its operators harbored no illusions about the substantial technical complexity of this experiment, we were somewhat surprised by the downright finicky nature of the apparatus. This could have been foreseen from the increased infrastructure (added to the already substantial complexity of the apparatus described in chapters 2 and 3), but we soon found the sensitivity of the locking chain described in Figure ?? to be the largest impediment to forward progress. Operating the system required much longer start-up time than the pure millitrap work, and for many months  $\sim 2$  all-nighters per week became the norm as the system appeared to retain lock for longer stretches of time if the *clock* time was single digits, followed by A.M. While many missteps were made and many confused debates were conducted in the wee hours of the morning, at the time of this writing the system appears very well understood (as evidenced by the two papers referenced above). While the definitive word on the new physics which will be borne out of BEC-CQED system awaits documentation in other theses, this chapter follows (somewhat chronologically) the critical experiments which allowed us to understand the unique system we had implemented.

## 7.1 Atom Transits

The first step in any cavity QED experiment is the observation of atom “transits” through the cavity by the change in the cavity transmission. The atoms will ultimately be precisely delivered to the cavity mode, but to begin the cavity mode must be located. The cavity was thereby tuned to resonance and we blindly moved the atoms through the cavity while monitoring the cavity transmission. After some trial and error in the transverse positioning of the atom trajectory, the signal shown in Figure 7.1 was observed.

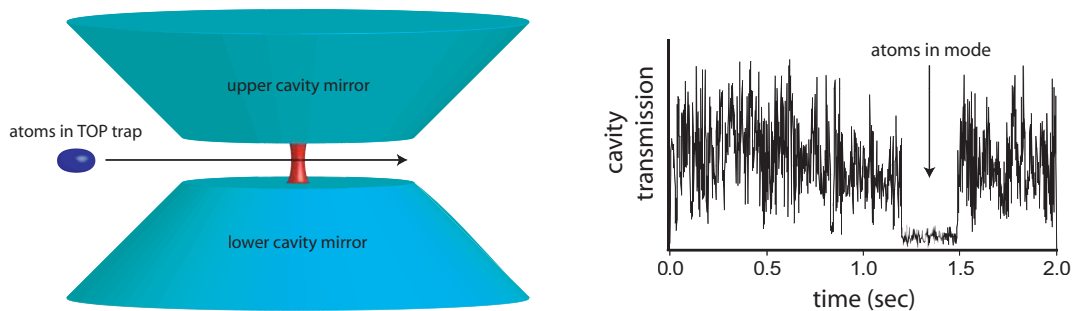


Figure 7.1: Observation of controlled atom transits. As shown in the sketch on the left, the TOP-trapped atoms are brought through the cavity mode. As seen in the cavity transmission, the presence of the atoms in the mode shifts the resonance away. After the atoms have left the mode, the transmission returns to its previous level.

With this signal in hand, the precise spatial position of the cavity mode could be determined via cavity transmission alone. Ultimately we would gain another method by which to “see” the mode, but this must await a later section.

## 7.2 Probing the Shifted Cavity

As reliably transferring ultracold atomic clouds (initially bound in the TOP trap) into the cavity mode became commonplace, a new language began to emerge as we dutifully recorded “uptick times,” searched far and wide for the “the line,” and dreamt lofty goals of publishing a PRL entitled simply “Quantum Upticks.” While obscure to outside observers, these phenomena became familiar to us as our first window in the dynamics of the many-

atom cavity system, and surely deserve a detailed exploration here.

### 7.2.1 Upticks

As seen in the atom transit graph of Figure 7.1, the cavity is rapidly shifted out of resonance as atoms are introduced to the cavity mode. The hard edge which is seen as the cavity comes back into resonance, however, is caused in this case by the fact that the atoms are removed from the cavity mode as quickly as they arrived while the cloud follows a constant velocity trajectory.

Far more interesting is the case where the atoms are placed in the cavity mode and are removed from the system through other mechanisms. We defer a detailed discussion of the loss induced by the cavity probe (both off- and on-resonance) [144], but at the very least the number loss due to background gas collisions is omni-present. As these losses take the atom number in the mode  $N \rightarrow 0$ , the cavity shift  $\Delta_N = \frac{Ng_{eff}^2}{\Delta_a}$  will be tuned back to  $\Delta_N = 0$ . For the experimentalist monitoring the transmission of the cavity with probe tuned to the unshifted cavity resonance ( $\Delta_c = 0$ ), the CRVC output will resemble the data stream presented in Figure 7.2(b).

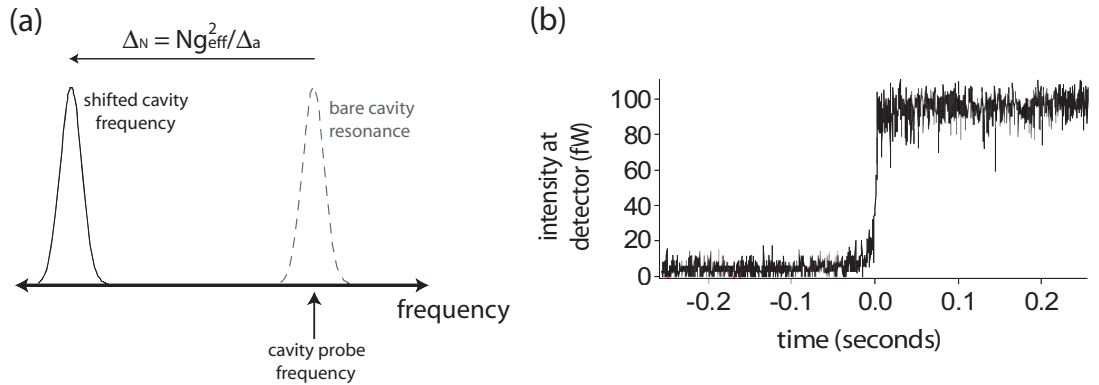


Figure 7.2: Upticks (a) Frequency-space picture of the uptick process. Atoms are loaded into the cavity ODT, shifting the cavity from resonance by  $\Delta_N = Ng_{eff}^2/\Delta_a$ . Light resonant with the empty cavity is impinged upon the system, but is reflected due to the  $\Delta_N$  shift. As the atoms are depleted from the trap, the cavity is brought back into resonance, finally sparking full transmission as seen in (b).

The time delay between the initiation of the probe and the moment at which the cavity

transmission spikes back to its “empty cavity” level is known as the uptick time. With a weak probe ( $\Gamma_{meas} = 10^5$  /s,  $\bar{n} = 0.24$ ), uptick times of  $> 40$  seconds were observed. Shortened uptick times spoke to either poor atom number population (which could be confirmed by absorption imaging) or an increased atom loss rate. The increased atom loss rate could speak to higher chamber pressure or, far more likely, some light-induced losses from the action of the probe. There are some important subtleties for off-resonance probe losses which will be revisited later in this chapter.

### 7.2.2 The Stationary Probe

Measuring the cavity shift  $\Delta_N$  of course involves tuning the probe away from the bare cavity resonance. Two types of experiments which explore the cavity shift are possible, both with their own virtues. The first is the “stationary probe,” which is closely related to the uptick measurements and is depicted in Figure 7.3.

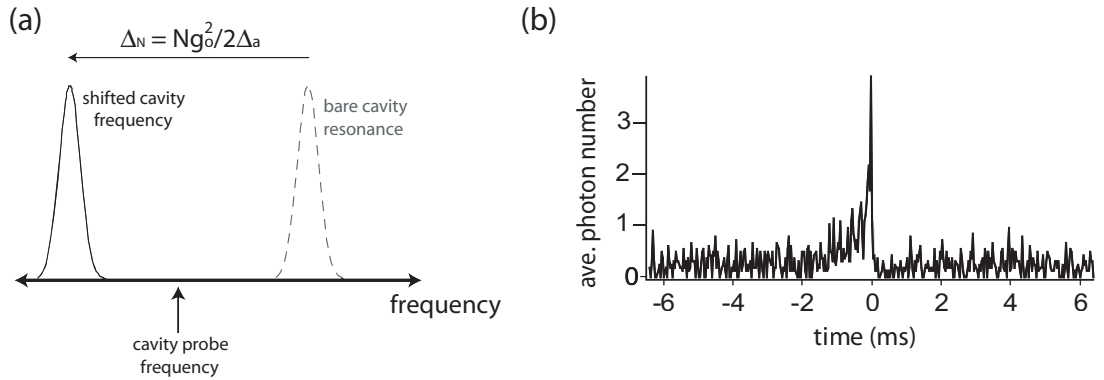


Figure 7.3: Cavity Line Transits with Stationary Probe. (a) Similar to the uptick process, the cavity is shifted by the presence of the atoms, but the probe is now tuned between the shifted cavity and the bare cavity. (b) As the atoms are depleted the cavity is brought into resonance for a brief time, and then tuned away from resonance as the system returns to the empty cavity resonance. The atomic detuning in this case was  $\Delta_a = -2\pi \times 300$  GHz.

For these stationary probe experiments, the cavity probe is detuned from the bare cavity resonance by  $\Delta_c = \omega_p - \omega_c$ . With  $N$  intracavity atoms in the dispersive limit, the cavity shift is  $\Delta_N = Ng_{eff}^2 / \Delta_a$  and is presumably greater than  $\Delta_c$ . As atoms are lost from the system,  $\Delta_N$  will steadily be reduced until it approaches and equals  $\Delta_c$ . Up to

this point, the probe light which was incident upon the cavity was mostly reflected as the lorentzian lineshape dictates the transmission to be  $(1 + \frac{(\Delta_c - \Delta_N)^2}{\kappa^2})^{-1}$  off-resonance. As  $\Delta_c \approx \Delta_N$  within  $\kappa$ , the transmission spikes as the resonance condition is met and the intracavity light field is built up. The presence of  $\lambda_p \approx 780$  nm light in the cavity causes heating which accelerates the atom loss [144]. This will rapidly take the system from  $\Delta_N > \Delta_c$  to  $\Delta_N < \Delta_c$ , and the observation at the photodetector will be a “line” which represents the photons which passed through the cavity for the brief time when  $\Delta_N \approx \Delta_c$ .

As the value of  $\Delta_c$  is set by the experimentalist, the arrival of the line is in fact a measurement of the atom number from  $N = \frac{\Delta_g \Delta_c}{g_{eff}^2}$  (on resonance). This hypothesis may be tested by triggering an absorption image on the arrival of the line, and the linear correlation between the cavity shift and the number count in Figure 7.4(b) not only confirms the theory but also provides an independent measurement of  $g_{eff}^2$ . For the data shown in Figure 7.4(b), the data confirm the expected value of  $g_{eff}^2 = \frac{1}{2} \times \frac{5}{6} \times (2\pi \times 15.6 \text{ MHz})$ . The  $\frac{1}{2}$  factor is of course from spatial averaging, the 15.6 MHz conforms to the expected value of the cavity coupling from the knowledge of the mode volume, and the  $\frac{5}{6}$  factor arises from the  $\sigma^+$  polarization of the probe light.

### 7.2.3 The Chirped Probe

The second method of probing the cavity shift involves operating the probe in “sweep” mode, where the cavity detuning  $\Delta_c$  is swept linearly in time across  $\Delta_N$ . This situation is perhaps more controlled than the passive line transits of the stationary probe, as in the sweep experiments the probe level and sweep rate are determined by the experimentalist. In particular, the probe power can be reduced to such a level that the traversal of the line (and corresponding dose of optical power) hardly influences the atom number after sweeping through resonance, yielding a “non-destructive” probe of the atom number. The relation of this non-destructive nature to the topic of quantum non-demolition (QND) measurements will be discussed in a subsequent section, but for the purposes of this discussion the technique may be thought of as an alternative measurement of the atom number akin to phase-contrast imaging [21] in its weak effect on the atom population. The sweeping method is depicted in Figure 7.5.

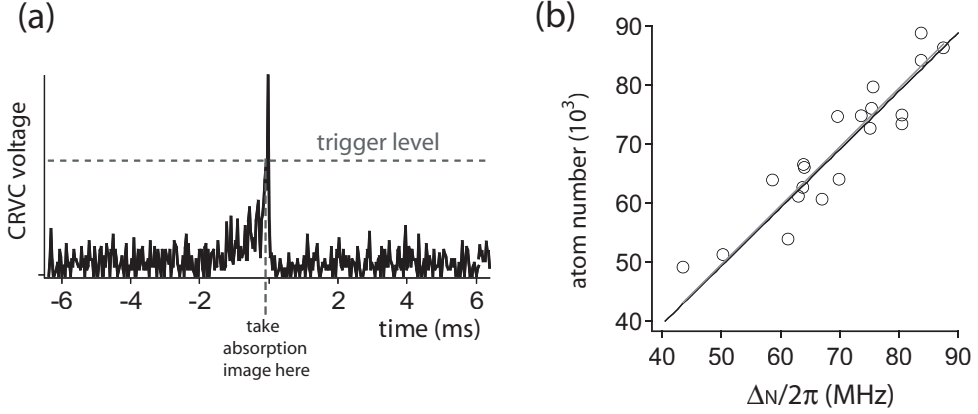


Figure 7.4: Cavity line shift as a number measurement. (a) The CRVC output is set to trigger an absorption image at a certain count rate corresponding to  $\Delta_c \approx \Delta_N$ . (b) The absorption images provide an independent measurement of the atom number, and for a set of such experiments with  $\Delta_a = 2\pi \times (100\text{GHz})$  the number count from the triggered absorption images are plotted against the  $\Delta_N$ . There is not one but two lines through the data, with the black line representing the slope predicted by the expected  $g_{eff}^2 = \frac{1}{2} \times \frac{5}{6} \times g_m^2 = (2\pi)^2 \times 104\text{MHz}^2$  and the grey line the least squares fit to the data (with a constrained zero crossing). The fit gives the measured value of  $g_{eff}^2$  to be  $(2\pi)^2 \times 99\text{MHz}^2$ , 5% off the expected value. The noise on the absorption imaging measurements were at least at this level due to poor image quality from light diffraction off the mirror edges, so this should be interpreted as a confirmation of our hypothesis within the experimental precision.

### 7.3 FORT in the Cavity

While the primary function of the 850 nm laser is to lock the cavity length, it boasts a second and remarkably useful function: that of a Far-Off-Resonance optical Trap (FORT) [145]. The advantages of optical trapping in a cavity are many, but perhaps none as much as the “state independent” nature of the trapping [41]. Optical trapping opens the possibility of probing ensemble spin dynamics with the cavity, a scenario which is precluded by a magnetic trap and explored later in this chapter.

The theory behind optical trapping is explored in great detail elsewhere [20, 63, 146, 147]. The AC Stark shift of the ground state for a far-detuned  $\pi$ -polarized beam of intensity

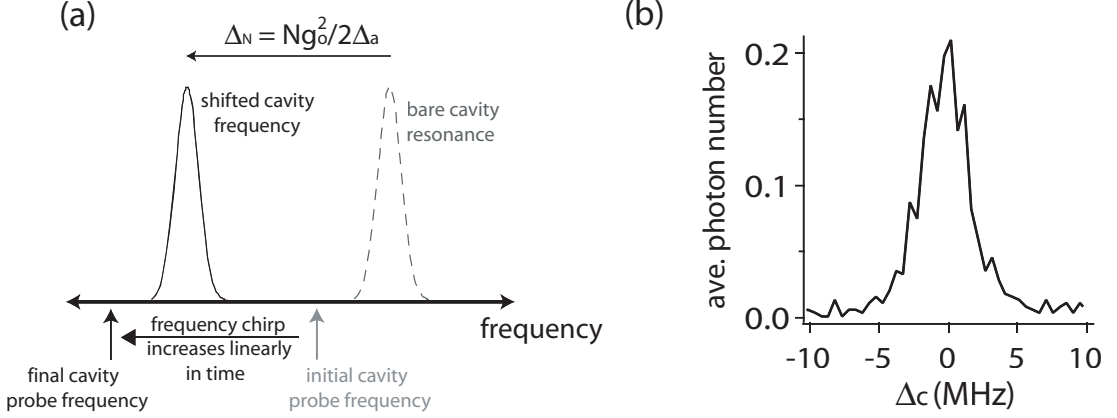


Figure 7.5: Sweeping the probe over the shifted cavity resonance. (a) Unlike the passive process of Figure 7.3, the probe is chirped in time such that it sweeps across the shifted cavity resonance. (b) A

$I$  incident upon a  $^{87}\text{Rb}$  atom is given by

$$\Delta E_g = \frac{\hbar\gamma^2}{8} \frac{I}{I_{sat}} \left( \frac{1}{3} \frac{1}{\delta_{D1}} + \frac{2}{3} \frac{1}{\delta_{D2}} \right), \quad (7.1)$$

where  $I_{sat} = 1.4 \text{ mW/cm}^2$ ,  $\delta_{D1}$  and  $\delta_{D2}$  are the detunings of the beam from the  $D1$  and  $D2$  lines (the  $\frac{1}{3}$  and  $\frac{2}{3}$  factors are from the Clebsch-Gordan coefficients for the transitions).

The optical power inside the cavity  $P_c$  is discerned from the output power  $P_{out}$  by  $P_c = \mathcal{F}_t P_{out} / \eta_t$ , where  $\eta_t$  is the efficiency budget for the 850 nm light  $\eta_t = \frac{1}{2} \times \frac{0.66}{\times} 0.8 = 0.26$ , where the factors were the balanced cavity, the dichroic mirrors, and the interference filter, respectively. The maximum AC stark shift in the cavity is thus given by

$$\Delta E_g = -k_B \times 65 \times \left( \frac{P_{out}}{nW} \right) nK. \quad (7.2)$$

As the mode structure inside the cavity is of the form  $|\phi(\mathbf{r})|^2 \propto \sin^2(k_t z) e^{-\rho^2/w_t^2}$ , the conversion to the trapping frequencies of the wells of the optical potential is given by:

$$\omega_z = 2\pi \times 4.1 \times 10^3 \times \sqrt{\frac{P_{out}}{nW}} \text{ Hz} \quad (7.3)$$

$$\omega_\rho = 2\pi \times 32.5 \times \sqrt{\frac{P_{out}}{nW}} \text{ Hz}. \quad (7.4)$$

While these conversions come from the theoretical equations, they were ultimately confirmed experimentally.

This is not the first standing wave FORT inside a cavity to trap cold atoms [41], but it is the first instance where atoms are controllably delivered *pre-cooled* to an intracavity FORT. Loading the atoms into the FORT was complicated by the fact that the intracavity optical power couldn't be arbitrarily lowered without losing the cavity lock. The lowest level which we would maintain lock was effected an AC Stark shift of  $\Delta E_g \sim -k_B \times 100$  nK, well below the  $4E_{rec} = k_B \times 710$  nK level at which the FORT cannot support bound states, so its effect can be ignored other than a modification of the effective mass. The  $1 \mu\text{K}$  level is approximately the temperature of atoms which will be placed into the cavity region from the TOP trap. While the "sky's the limit" on the largest Stark shift possible, other detrimental effects enter in such as increased three-body losses and enhanced heating from the ODT power fluctuations.

Loading the atoms was optimized through a sequence which lowered the FORT to  $\sim 1 \mu\text{K}$ , aligned the TOP-trapped atoms with the cavity mode, and then terminated the magnetic trap and, over the course of  $\approx 1$  ms, increased the FORT depth to  $6 \mu\text{K}$ . While some atoms were lost in the transfer process, the loading was  $> 25\%$  efficient. The loading process is depicted in Figure 7.6(a), including an image of  $\sim 10^5$  atoms trapped in the FORT.

As the  $6 \mu\text{K}$  trap was typical, it is instructive to consider some thermodynamic quantities of interest. With similarly typical loading conditions, we can consider placing 100,000 atoms evenly distributed over 300 sites, meaning each lattice site holds approximately 300 atoms. Finally, observed temperatures<sup>1</sup> consistently showed  $\sim 0.8 \mu\text{K}$  temperatures for the optically trapped atoms. Table 7.3 summarizes relevant energetic and thermodynamic quantities.

A few facts stand out from Table 7.3. First, the ground state energy of the axial trap is  $\frac{1}{2}\hbar\omega_z \approx 1 \mu\text{K}$ , almost exactly the observed temperature. Thus, the atoms will primarily be found in the axial ground state and are thermally distributed amongst the transverse harmonic states. Second, the evaporation parameter  $\eta = U_o/k_B T = 6$  is very

<sup>1</sup>These were measured in the brief time of flight imaging available when the cavity FORT is extinguished and the atoms fall under gravity. With less than  $100 \mu\text{m}$  to fall before the majority of the cloud is obscured by the lower cavity mirror, no more than 4 ms of free fall time was available. Temperatures were estimated from the growth of the transverse width, though the data were rather noisy due to the diffraction of imaging light off mirror edge.

$k_t$ : Cavity FORT wavevector .....	$2\pi/850$ nm
$w_t$ : TEM <sub>00</sub> mode waist for 850 nm .....	$24.4$ $\mu$ m
$N_s$ : Atom number per site .....	$\sim 300$
$U_o$ : Trap depth .....	$5$ $\mu$ K
$T$ : Temperature .....	$0.8$ $\mu$ K
$\eta$ : Evaporation parameter, $\frac{U_o}{k_B T}$ .....	$6$
$\omega_z$ : Axial trapping frequency, $k_t \sqrt{\frac{2U_o}{m}}$ .....	$2\pi \times 40$ kHz
$\omega_\rho$ : Transverse trapping frequency, $\frac{2}{w_t} \sqrt{\frac{U_o}{m}}$ ....	$2\pi \times 310$ Hz
$\sigma_z$ : Axial width (rms), $\sqrt{\frac{2\hbar}{m\omega_z}}$ .....	$70$ nm
$\sigma_\rho$ : Transverse width (rms), $\frac{1}{\omega_\rho} \sqrt{\frac{k_B T}{m}}$ .....	$12$ $\mu$ m
$n$ : Density, $N_s/\sigma_z\sigma_\rho^2$ .....	$3 \times 10^{13}$ cm <sup>-3</sup>
$g$ : Interaction strength, $\frac{4\pi n\hbar^2 a_s}{m}$ .....	$2\pi \times 210$ Hz
$T_c$ : BEC transition temperature, $\approx \hbar\bar{\omega}N_s^{1/3}/k_B$ .....	$0.5$ $\mu$ K
$\Gamma_c$ : Collision rate, $n(8\pi a_s^2)\sqrt{\frac{k_B T}{m}}$ .....	$500$ Hz
$\Gamma_t$ : Tunneling rate, $\approx \omega_z e^{-\lambda_p} \sqrt{2m(U_o - \hbar\omega_z)}/2\hbar$ ...	$0.02$ Hz
$\eta_{LD}$ : Lamb-Dicke parameter, $k_p\sigma_z$ .....	$0.28$

Table 7.1: Optical lattice parameters

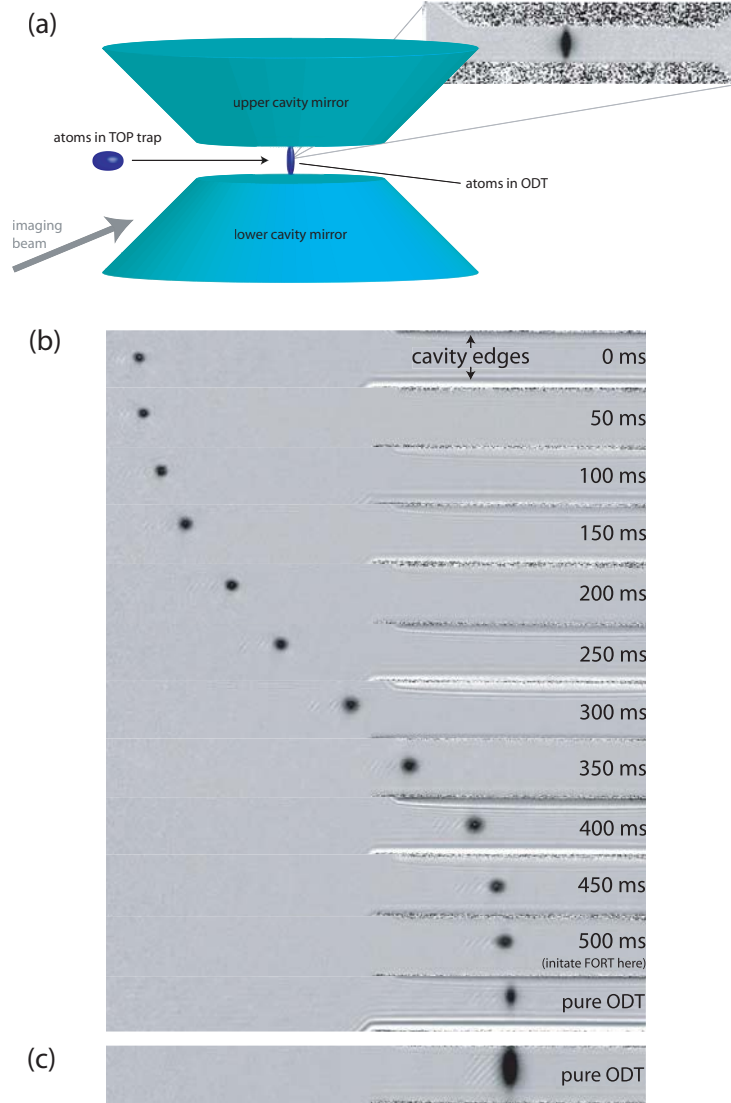


Figure 7.6: Loading atoms into the cavity FORT. (a) Diagram shows the transfer of atoms from outside to inside the cavity, with the imaging axis shown. (b) In-trap images of a condensate being loaded into the ODT of the cavity. The TOP minimum is smoothly shifted from outside the cavity to inside over 500 ms, and then finally loaded into the ODT as described in the text. (c) A much larger ODT population in the cavity FORT is seen by the loading of a  $1\mu\text{K}$  thermal cloud.

noteworthy, as typically during forced rf evaporation towards BEC this parameter is held at  $\approx 10$ . Finally, that the ratio of  $T/T_c = 1.6$  is so close to 1 raises the possibility of Bose condensation in each lattice site. As  $T_c \propto U_o^{1/2} \times N_s^{1/3}$ , modest enhancements could

readily bring the transition temperature to  $1\ \mu\text{K}$ . The trap depth was particularly easy to increase, but even we operated the system with  $U_o > 20\ \mu\text{K}$  (nominally,  $T/T_c = 1.1$ ) we did not observe any signature of condensation. Further improvements are well within the realm of possibility, and this remains a subject surely worth further investigation.

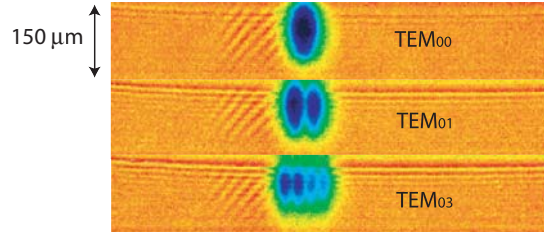


Figure 7.7: Ultracold atoms as intracavity power meters. The cavity is locked to different transverse modes of the 850 nm locking/trapping light, and the atoms are loaded from the TOP as in Figure 7.6. The higher order TEM modes show the characteristic Hermite polynomial shape, with a slight bias in population on the loading side.

While this apparatus was designed to magnetically confine atoms in the cavity mode, utilizing the FORT to confine the atoms has proven to be the most useful experimental avenue. One reason for this is the fact that each well of the standing wave potential is in the regime where the Lamb-Dicke parameter  $\eta_{LD} = k_p \sigma_z = 0.28$  for the  $6\ \mu\text{K}$  FORT. The “Lamb-Dicke regime” is the case where  $\eta_{LD} < 1$ , and in the context of cavity QED this implies that each site in the optical lattice has a well-defined cavity coupling. The value of each well coupling is easily calculated by the beat note between the 850 nm trapping light and the 780 nm probe light. The coupling is thus approximately periodic over  $4.7\ \mu\text{m}$ , or  $\sim 11$  lattice sites, which is depicted in Figure 7.8.

## 7.4 Splitting the Cavity Shift with Atomic Polarization

It is likely to be the case that the TOP-to-ODT transfer will retain the entire population in the  $|F = 1, m_F = \pm 1\rangle$  state. With this known atomic polarization, we may verify the effect of light polarization on the cavity shift. In the dispersive limit, the hyperfine energy splittings are irrelevant and a look at the Clebsch-Gordon coefficients (presented in Figure 6.1) for the D2 transitions shows how the polarization will affect the line splitting.

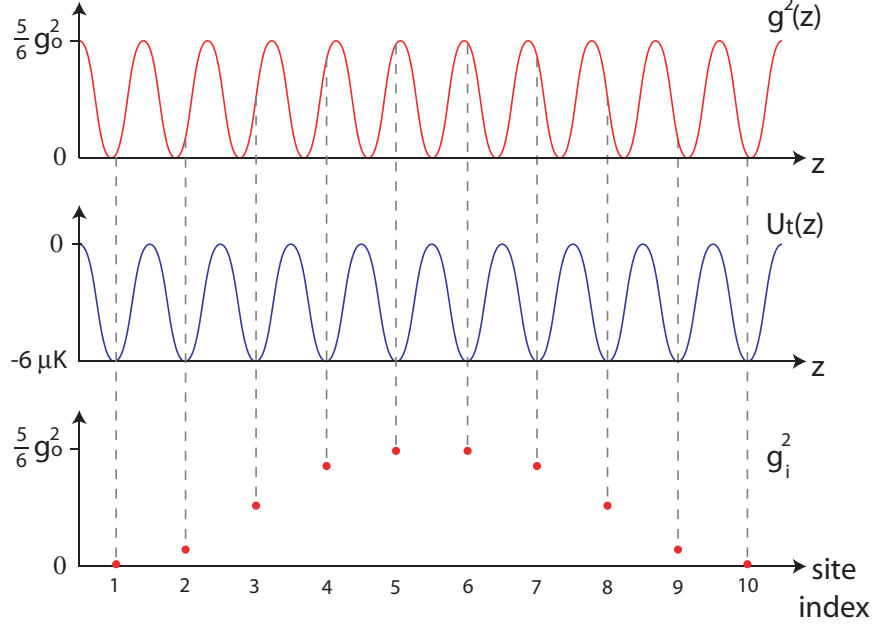


Figure 7.8: The axial variation of the cavity coupling  $g^2(z)$  (red) is compared with the axial variation of the optical trap potential  $U_t(z)$ . Atoms are confined to the minima of  $U_t(z)$ , and for atoms well-localized in these minima each well will have a specific value of  $g_i^2$  as shown.

The sum of the squared coefficients for each transition gives the coefficient on the cavity shift, i.e.  $\Delta_N \rightarrow \left(\frac{5}{6}\right) \frac{Ng^2}{\Delta_a}$  in the case of  $\sigma^+$  polarization and  $\Delta_N \rightarrow \left(\frac{1}{2}\right) \frac{Ng^2}{\Delta_a}$  in the case of  $\sigma^-$  polarization.

Presented in Figure 7.9 is a stationary probe trace for the system with a linearly polarized probe, which of course consists of equal parts  $\sigma^+$  and  $\sigma^-$ . *Two* lines are seen as two different values of the atom number satisfy the  $\sigma^+$  resonance condition ( $\Delta_c = \frac{5}{6} \frac{N_+g_0^2}{2\Delta_a}$ ) and the  $\sigma^-$  resonance condition ( $\Delta_c = \frac{1}{2} \frac{N_-g_0^2}{2\Delta_a}$ ). The  $\sigma^-$  is seen first, as its resonance occurs with  $1.5\times$  the atom number of the  $\sigma^+$  resonance. This line splitting may be used to verify the polarization character of the probe, which may differ from the “on-the-table” polarization due to cavity birefringence (though we did not observe this). The fact that the  $\sigma^+$  trace in Figure 7.9 shows only one discernable line is compelling evidence that other spin states remain unpopulated in the transfer to the cavity FORT, but *definitive* experimental evidence for this must await a later section.

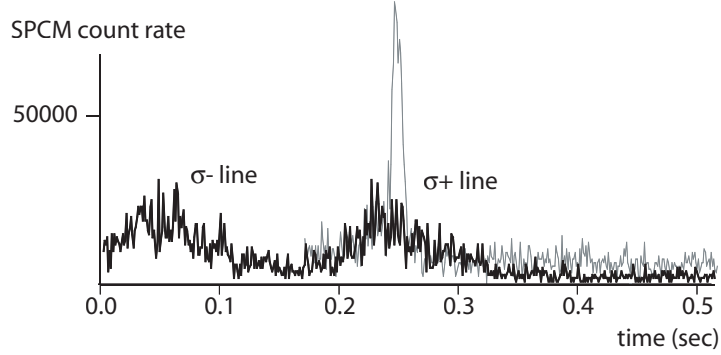


Figure 7.9: Line Splitting with a linearly polarized probe for  $\Delta_a = 2\pi \times (-80\text{GHz})$ ,  $\Delta_c = 2\pi \times (-5\text{MHz})$ . Shown are stationary probe traces for a  $\sigma^+$  polarized probe (grey) and a linearly polarized probe (black). The distinctly different widths and heights actually portended recent work cavity heating [144] and nonlinear optics [148].

## 7.5 Hybrid Trap

One novel functionality of the apparatus came when the atoms confined in the TOP trap were overlapped with the cavity mode while intracavity locking/trapping light was also engaged at a level sufficient to trap the atoms. We came to call this dual trapping scenario the “hybrid trap,” and while it is not immediately interesting as a testbed for many-atom cavity QED, it is instructive to consider the dynamics of the hybrid trap. It also highlights the atomic polarization sensitivity of the cavity, which leads to the introduction of a new data analysis technique explored in the subsequent section.

In the hybrid trap the majority of the atoms are confined entirely in the TOP (very weakly coupled to the cavity), but a fraction of the atoms are confined by both the TOP and FORT (strongly coupled to the cavity). There is no motional dissipation, so this conservative system assures that the populations will be exchanging particles at a rate at roughly the transverse trapping frequency of the TOP trap. This situation is depicted in Figure 7.10(a).

Investigating this system with a stationary detuned probe shows this system to behave quite differently than the lines observed for atoms in the FORT. As seen in Figure 7.10(b), the line is much longer in duration and heavily asymmetric on the “outgoing” side (when atom loss is tuning the cavity shift *away* from resonance). This asymmetric line may be

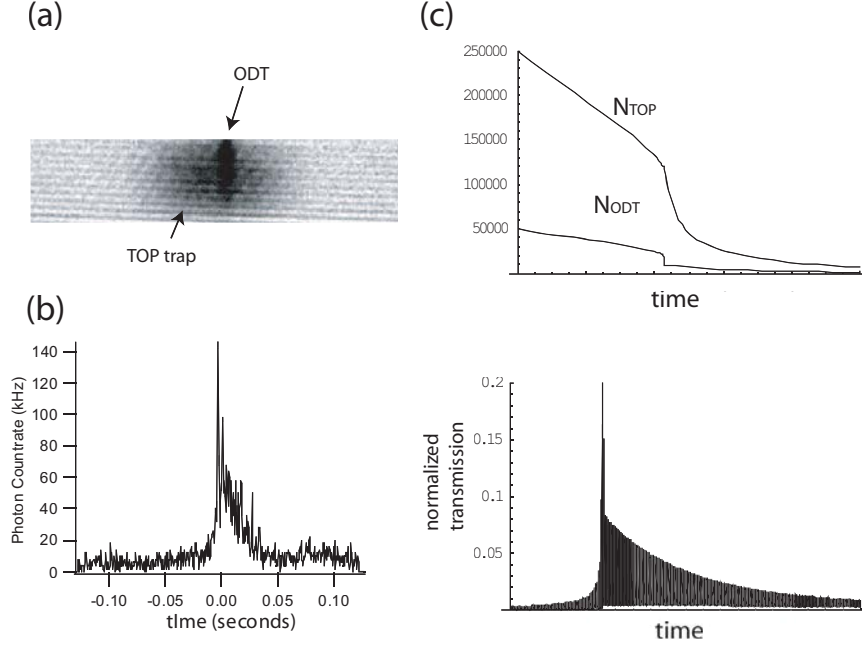


Figure 7.10: The hybrid trap. (a) Absorption image of the hybrid trap, with both TOP trapped atoms and ODT trapped atoms. (b) Stationary probe at a detuning of  $\Delta_a = 2\pi \times (-5.7\text{GHz})$  shows a line biased to the “outgoing” side. (c) Numerical models described in text account for the TOP and ODT populations ( $N_a$  and  $N_2$ , respectively) in time. (d) The same model (at high bandwidth  $\gg \omega_r$ ) shows the cavity transmission to qualitatively match the observed output, with a heavy modulation at  $\omega_r$ .

understood in the context of a simple two population model involving  $N_1$  (the atoms in the cavity) and  $N_2$  (the atoms outside the cavity but still bound by the TOP trap). Both populations suffer a homogeneous loss rate  $\lambda_H$  from background losses. The populations exchange particles at a rate  $\sim \omega$  (the transverse TOP trapping frequency) and the nominal ratio of the populations is  $f = \frac{N_2(t=0)}{N_1(t=0)}$  (this will depend on a number of factors including trap volume, temperature, cavity mode size, FORT intensity, etc.). Finally, the population  $N_1$  is susceptible to loss due to the intracavity photons, given by a per-atom loss rate of  $\alpha/(1 + \frac{(\Delta_c - \Delta_N)^2}{\kappa^2})$ .  $\alpha$  is a coefficient predicted by cavity heating models (see the last section of this chapter), and the Lorentzian lineshape of the cavity quantifies the number of intracavity photons for a constant input flux<sup>2</sup>. Finally, the action of the TOP field

<sup>2</sup>Recent investigations presented in Ref. [144] show that this should in fact be the Voigt profile, a convolution of the Lorentzian cavity lineshape and a Gaussian probe. Incorporating this into the present analysis would not give qualitatively different results, and qualitative features are all this model is expected

must be considered. Under a probe circularly-polarized along the cavity axis, the orbiting TOP field orients the  $|F = 1, m_F = -1\rangle$  atoms along (effectively  $\sigma^+$  polarization) and against (effectively  $\sigma^-$  polarization) the cavity axis, yielding respective squared couplings of  $\frac{1}{2}\frac{g_o^2}{2}$  and  $\frac{5}{6}\frac{g_o^2}{2}$ . This implies that the cavity shift is oscillating at the TOP frequency as  $\Delta_N = \frac{N_1 g_o^2}{2\Delta_a} \left(\frac{2}{3} + \frac{1}{6} \sin \omega_r t\right)$ .

With this we can construct a first-order model of the hybrid trap lineshape under a stationary probe. The coupled differential equations for this simple model are:

$$\dot{N}_1 = -\Gamma_H N_1 + \omega (f N_2 - N_1) - \alpha \left( 1 + \frac{\left( \Delta_c - \frac{N_1 g_o^2}{2\Delta_a} \left( \frac{2}{3} + \frac{1}{6} \sin \omega_r t \right) \right)^2}{\kappa^2} \right)^{-1} N_1 \quad (7.5a)$$

$$\dot{N}_2 = -\Gamma_H N_2 - \omega (f N_2 - N_1) \quad (7.5b)$$

which are numerically integrated in and displayed in Figure 7.10(c). The cavity output is proportional to  $\left[ 1 + \left( \Delta_c - \frac{N_1 g_o^2}{2\Delta_a} \left( \frac{2}{3} + \frac{1}{6} \sin \omega_r t \right) \right)^2 / \kappa^2 \right]^{-1}$  and is the observed quantity at the photodetector. The cavity transmission for the numerically integrated equations in Equations 7.5a and 7.5b are shown in 7.10(d) with the same asymmetric lineshape seen in the data. Briefly stated, the reservoir of  $N_2$  atoms streaming into  $N_1$  provides a source term on  $\Delta_N$ , which is otherwise a monotonically decreasing quantity. This was initially thought to be a situation of negative feedback where, for a time, the source term  $\omega f N_2$  was balanced by the losses. This would not hold  $N_1$  constant, as  $N_2$  is obviously decreasing as well, but the line would be “stretched” until the  $N_2$  reservoir is so depleted that the  $N_1$  loss rate returns to  $\approx \lambda_H$ . In the presence of the fast TOP frequency  $\omega_r$  this picture is muddied further, and the hybrid line is perhaps better thought of as merely a complex interplay between the reservoir  $N_2$ , the inhomogeneous cavity losses on  $N_1$ , and the now oscillating  $\Delta_N$ .

One upshot of this complex system is the fact that the line is now 30 ms long as opposed to 1 ms, the overall signal for a hybrid line is substantially greater than that of the FORT line from sheer photon counts. In particular, the harmonic drive  $\omega_r$  on the cavity coupling should be evident in the data stream, and by taking the fourier power spectrum of the raw SPCM data stream associated with the hybrid line shown in Figure 7.10(b), we obtain the graph in Figure 7.11 with a prominent and familiar frequency component.

to provide.

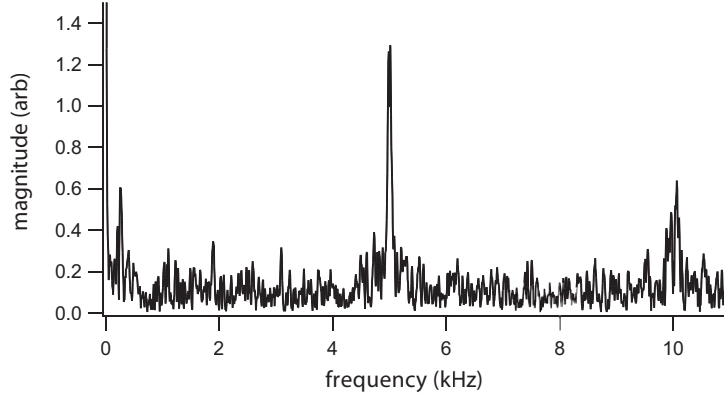


Figure 7.11: Fourier transform power spectrum of a hybrid line. The 5 kHz TOP frequency is picked up as a modulation on the cavity shift. (The power spectrum is obtained by taking the fourier transform of the SPCM data stream.)

## 7.6 Cavity Fourier Transform Spectroscopy

At this stage, Figure 7.11 is merely a measurement of the (already known) TOP frequency, but this “cavity fourier transform spectroscopy” on the internal state of the atoms will prove itself even more useful when considering the far more interesting cases of Larmor precession. It can also be employed in the case of collective atomic motion, as a coordinated reorganization of the  $N$  atoms in the cavity can take the cavity shift from  $\Delta_N = \frac{5}{6}Ng_0^2$  for the atoms all located at  $\lambda = 780$  nm cavity anti-nodes,  $\Delta_N = 0$  for the atoms all located at  $\lambda = 780$  nm cavity nodes.

The concept of cavity fourier transform spectroscopy also relates to the correlation function of the cavity transmission, which has been the preferred method for measuring photon anti-bunching [42] and even counting statistics of atom lasers (as measured by a strongly-coupled cavity) [50]. The first-order correlation function is defined as  $G^{(1)}(\tau) \equiv \int_{-\infty}^{\infty} dt f^*(t)f(t + \tau)$ . In this case,  $f(t)$  is the TTL output of the SPCM, which was of course the source of the fourier transform power spectrum shown in Figure 7.11. A few lines of algebra yields the connection of the correlation function to the fourier transform spectrum.

$$\begin{aligned}
G^{(1)}(\tau) &= \int_{-\infty}^{\infty} dt f^*(t)f(t+\tau) \\
&= \int_{-\infty}^{\infty} dt \left( \int_{-\infty}^{\infty} d\omega F^*(\omega)e^{-i\omega t} \right) \left( \int_{-\infty}^{\infty} d\omega' F(\omega')e^{i\omega'(t+\tau)} \right) \\
&= \int_{-\infty}^{\infty} d\omega \int_{-\infty}^{\infty} d\omega' F^*(\omega)F(\omega')e^{i\omega'\tau} \int_{-\infty}^{\infty} dt e^{i(\omega'-\omega)t} \\
&= \int_{-\infty}^{\infty} d\omega \int_{-\infty}^{\infty} d\omega' F^*(\omega)F(\omega')e^{i\omega'\tau}\delta(\omega-\omega') \\
&= \int_{-\infty}^{\infty} d\omega |F(\omega)|^2 e^{i\omega\tau}, \tag{7.6}
\end{aligned}$$

which is of course just the inverse fourier transform of the square of the fourier transform of  $f(t)$ . Thus, all the information in the fourier transform power spectrum is accessible via the correlation techniques of Refs. [42, 50], and vice versa.

## 7.7 Sub-“Shot Noise” Number Counting

That a measurement of the cavity resonance directly relates to a measurement of the atom number immediately invites the question as to how precisely the ensemble population could be determined. If we presuppose the ideal initial condition of a coherent state of number and phase for the ensemble<sup>3</sup>, then Poissonian statistics are expected and the atom number uncertainty is given by  $\Delta N = \sqrt{N}$ . Using the previously-described “non-destructive” probe to initialize the system at  $N = 24,000$  atoms, we found that we could trigger on and then measure the atom number to a precision of  $\Delta N = 95$  atoms. This is well below the predicted “shot noise” value of  $\Delta N = 155$  atoms. As this method appears akin to spin squeezing techniques [150], it is instructive to consider whether such cavity transmission measurements achieve a Heisenberg-limited determination of the atom number.

For the following reasons, we claim that this method does *not* represent number squeezing of the atom population, and the arguments herein apply to any other quantum variable (e.g. position, momentum, or spin) to which the atom-cavity system is sensitive.

---

<sup>3</sup>There is no *a priori* reason to expect the system to be in a coherent state of number and phase, but this serves as the “ideal” initial state in the absence of more advanced preparation techniques [149].

First, we note that the measurement made was not directly measuring the atom number, but instead  $\sum_i N_i g_i^2$ , where  $i$  indexes the respective wells of the optical trap. As previously noted,  $g_i^2$  can vary from 0 to  $\frac{5}{6}g_o^2$  depending on the overlap of the 850 nm trapping potential with the 780 nm probe. Second, it is conceivable that instead of squeezing the atom number  $N$  that perhaps we are projecting the system into a subset of atom distributions which satisfy  $\Delta_N = \sum_i N_i g_i^2 / \Delta_a$ . While this is not an obviously a useful subset of states, it is composed of two quantum variables – number and position – which could be squeezed. Again we must assert that no squeezing has occurred because neither the atomic populations in the wells, nor the atoms which comprise them, have an *a priori* phase coherence. Thus, even if the atomic population were measured to a precision of one atom, the absence of either initial phase correlations or *in situ* mechanisms to establish phase correlations in the system preclude the possibility that we have yet accomplished any Heisenberg-limited measurement. The presence of cavity heating terms could further doom the prospects of cavity-enhanced Heisenberg-limited measurements; a discussion of these deleterious effects can be found in Ref. [144].